The native oxide film on a model aluminium-copper alloy studied by XPS and ToF-SIMS

P. Cornette, S. Zanna, A. Seyeux, Dominique Costa, P. Marcus

The native oxide film on a model aluminium-copper alloy studied by XPS and ToF-SIMS

P. Cornette,*[+], S. Zanna, A. Seyeux, D. Costa, P. Marcus*

Chimie ParisTech, PSL University, CNRS, Institut de Recherche de Chimie Paris, Physical Chemistry of Surfaces Group, 11 rue P et M Curie, 75005 Paris, France

Abstract:

Surface analytical techniques were used to characterize the chemical composition and the thickness of the surface oxide on an AlCu2.2%at alloy sample.

ToF-SIMS analyses show that the oxide layer is thinner on the intermetallic particles (IMPs) as compared to the Al matrix. Combined with XPS, analyses reveal that IMPs are covered by aluminium and copper(I) oxide whereas the Al matrix is covered by aluminium oxide. Moreover, metallic copper segregates at the oxide/metal interface on both matrix and IMPs.

The heterogeneities at the metal/oxide interfaces suggest that complex galvanic effects could occur between IMP and matrix substrate, and within the IMPs.

Keywords: Aluminium alloy; XPS; ToF-SIMS; Surface oxide

* corresponding authors:

pauline.cornette@chimieparistech.psl.eu

philippe.marcus@chimieparistech.psl.eu

[+] present address: Sorbonne Université, CNRS - UMR 7197, Laboratoire de Réactivité de Surface, 4 place Jussieu, F-75005, Paris, France.

1. Introduction

Aluminium alloys are widely used in aeronautics and aerospace applications.[1–3] Different alloying elements are used in order to improve mechanical properties. One of the most common alloying elements is copper and a variety of Al-Cu alloys have been developed (2000 serie). The addition of Cu alloyed elements leads to the formation of intermetallic Cu-rich particles (IMPs).[3,4] These IMPs are known to be at the origin of lower corrosion resistance of the aluminium alloys in aqueous chloride environments (pitting corrosion).[3,5–7]

On the Al rich-Cu alloys, the Al_2Cu IMPs are more noble than the surrounding matrix. Zhou *et al*.[8] report a corrosion potential of pure Al_2Cu of -473 mV//SCE whereas the one of Al is -507 mV/SCE in 0.1M Na_2SO_4. In 0.1M NaCl solution, Buchheit *et al*.[9] compiled different corrosion potentials and showed a potential at -665mV//SCE for Al_2Cu and -750mV//SCE for pure Al. Several publications[10–12] indicate that the corrosion potential is higher on Al_2Cu IMP than on pure Al before and after immersion in aqueous solution. Thus a galvanic cell can be formed between the matrix and the particles.[5] The Al_2Cu θ-phase particles act as cathode, providing more cathodic current for the reduction of oxygen, promoting the surrounding anodic matrix dissolution.[13–16] This can explain the localization of the pit initiation next to the particles, resulting in circumferential dissolution of the Al matrix (trenching). [5,6,17–19]

Inhomogeneities in the passive layers on Al and intermetallic particles are thought to enhance the susceptibility to pitting corrosion. Some studies report that the intermetallic particles have an impact on the thickness of the passive layer on the aluminium alloys.[20] It was reported that the copper containing particles oxidized at reduced rates relative to the Al matrix.[21]

It is known that both the matrix and the Al_2Cu intermetallic particles are covered by an aluminium oxide layer.[22–25] Whereas the oxide surface on pure Al has been largely characterized by surface analysis tools, the oxide covering the Al_2Cu phases has not been characterized to the same extent. Son *et al*.[26] observe a pure Al_2O_3 film on Al_2Cu substrate, without evidence of Cu oxidation as other authors[27]. Additional X-ray reflectivity and current-voltage measurements were conducted to characterize the electronic properties of the oxide on these $A1_2O_3/Al_2Cu$ thin films. The electron density and conductivity are both much higher than expected for pure $A1_2O_3$, suggesting that a small amount of a conductive impurity,

such as metallic Cu, may reside in the oxide layer. Other authors[28] suggest that the oxide formed on Al_2Cu is enriched in metallic Cu. Different studies[25,29] also demonstrated that the oxide layer on the IMP is thinner than on the matrix and composed of aluminium and copper oxide. Li *et al*.[25] also suggested that there was Cu enrichment at the metal/oxide interface.

The structure and composition of passive films is a key issue in corrosion science, including on Al alloys. In addition, for Al alloys containing Cu, the initiation of localized corrosion is often associated to the cathodic nature of the intermetallic particles, but the presence of an oxide layer at the IMP surfaces is largely ignored in the initiation mechanisms. A better knowledge of specific features of this oxide would be useful for understanding corrosion initiation mechanisms. We report here an experimental study of the oxide formed on Al-Cu2.2%at alloy. We characterize the local morphology, microstructure and chemical composition of the Al-Cu alloy surface, i.e. above the matrix and the IMPs. Time-of-Flight Secondary Ions Mass Spectrometry (ToF-SIMS) 3D images were recorded to have access, with a sufficiently good lateral resolution, to the regions corresponding to the matrix and the IMPs. Combined with X-ray Photoelectron Spectroscopy (XPS), the nature, composition and thickness of the oxide layers and the underlying metal layers are characterized. The goal of this work is to determine the surface composition above Al_2Cu particles and Al alloy.

2. Materials and methods

2.1 Sample preparation

A model alloy of aluminium/copper containing 4.87 wt % of copper (i.e. 2.2 at%), provided by GoodFellow, was cut into 1 cm^2 and 3 mm thick samples. The alloy sheets were first mechanically polished up to 2400 grade SiC paper, and then with water-based ESCIL® alumina suspension up to 0.3 µm. After polishing, the samples were successively sonicated in ultrapure water and ethanol for 2 minutes. The samples are then dried under a compressed air flow and stored overnight under ambient conditions. The samples are analysed the following day.

2.2 Chemical characterization

The surface chemical characterization was performed by means of XPS, ToF-SIMS and SEM-EDX, using a Thermo Electron ESCALAB 250 spectrometer, a ToF-SIMS V

spectrometer (ION TOF GmbH) and a ZEISSUltra-55 field emission scanning electron microscope, respectively.

For the X-ray Photoelectron Spectroscopy (XPS) analysis, the base pressure in the analysis chamber was $\sim 10^{-9}$ mbar. Al Kα monochromatized radiation (hν = 1486.6 eV) was employed as the X-ray source. The spectrometer was calibrated using the reference binding energies of clean Au $4f_{7/2}$ (84.1 eV) samples. For all analyses, the take-off angle was 90◦ and the analysed area was a 500 µm diameter disk. High resolution spectra of the C 1s, O 1s, Al 2s, Cu $2p_{3/2}$ and Al 2p core level regions were collected with a pass energy of 20 eV at a step size of 0.1 eV. Data processing (peak fitting and decomposition) was performed with the Avantage software provided by Thermo Electron Corporation, using an iterative Shirley-type background subtraction and Gaussian/Lorentzian peak shapes at a fixed ratio of 70/30. The binding energies are given with a ±0.1 eV uncertainty. Symmetrical peaks were used. Inelastic mean free path values (λ) were determined with the Tanuma Powell and Penn formula[30] except for aluminium values, which were adapted from the Marcus *et al.* calculation[31]. CasaXPS software (version 2.3.13) has been used to recombine the Cu Auger peaks using Cu(0), Cu(I) and Cu(II) reference Auger lines.

For the ToF-SIMS measurement, the chamber was operated at pressure below $\sim 10^{-9}$ mbar. The total primary ion flux was less than 10^{12} ions.cm^{-2} ensuring static conditions. All the analyses were recorded in the Burst-Alignment image mode (BA-IMAGE) in which the long primary pulse is burst into 4 shorter pulses to get good mass and lateral resolutions. The negative polarity (detection of negatively charged ions) has been chosen for a higher sensitivity to fragments coming from oxide matrices[32–39]. On the negative images, the characteristic ions of the surface are: Cu^-, CuO^-, AlO_2^-, and Al_2^-. They represent the metallic copper, the oxidized (oxide and/or hydroxide) copper, the oxidized (oxide and/or hydroxide) aluminium and the metallic aluminium, respectively. These ions are conventionally used to characterize Al-Cu alloy surfaces[29]. 3D chemical images (i.e. images at each sputtering depth) were recorded by interlacing a pulsed 25 keV Bi^+ primary ion source delivering 0.25 pA of target current over a 100 × 100 µm^2 area with sputtering using a 1keV Cs^+ source beam delivering 20 nA of target current over a 500 × 500 µm^2 area. The Bi^+ ion beam intensity is greatly reduced in order to limit the zone disturbed by the ions impact, which allows a good lateral resolution. With the chosen analysis conditions, the lateral resolution is well below 400 nm, thus good enough to observe the Al-Cu intermetallic particles present in the studied Al-Cu alloy. Data

acquisition and processing were performed using the IonSpec commercial software. The exact mass values of at least five known species were used for calibration of the data acquired in the negative ion mode.

For the SEM-EDX analysis, standard conditions were used to analyse Al-Cu alloy samples: an electron acceleration voltage of 15 kV, an electron beam current of the order of 180 pA and a pressure inside the chamber less than 10^{-6} mbar.

3. Results and discussion

3.1 Characterization of the intermetallic particles by SEM-EDX analyses

To determine the composition of the IMPs, the aluminium/copper model alloy samples, containing 2.2 at% copper, were analysed by scanning electron microscopy. An SEM image is shown in Figure 1. Intermetallic particles are uniformly distributed on the surface. Their diameters vary between 0.5 and 4 μm. The EDX analyses carried out on five samples reveal that the surface is essentially composed of aluminium at more than 99%at. The stoichiometry of the intermetallic particles is $Al_{2.7}Cu$ (average on 15 measurements). The depth of the SEM-EDX analysis is of the order of one micron. The detection of metallic aluminium coming from the matrix under the small particles (small diameters) cannot be neglected. Taking into account particles sufficiently large to limit the measurement uncertainty, a stoichiometry of $Al_{2.2}Cu$ is found, close to the stoichiometry of the stable phase θ-Al_2Cu. It can therefore be deduced that the intermetallic particles present in this model aluminium/copper alloy are Al_2Cu particles. This result is in agreement with literature which indicates that the θ-Al_2Cu phase is the stable equilibrium phase present in Al-Cu alloys.

3.2 In depth chemical composition of the alloy surface by ToF-SIMS analyses

ToF-SIMS 3D chemical analysis was conducted. This allows to extract, from the same set of data, a general depth profile (Figure 2) and 2D images at specific locations corresponding to (i) the extreme surface, (ii) the oxide film, and (iii) the metal/oxide interface (Figure 3).

On the general ion depth profile (Figure 2) the intensity of the ion signals (Cu^-, CuO^-, AlO_2^-, and Al_2^- recorded simultaneously), are plotted versus Cs^+ ion sputtering time. Ions intensity is reported in logarithm scale. Intensity changes with the sputtering time on the profile reflect in-depth concentration variations.

Three main regions can be identified. The first one, corresponding to the first 100s of sputtering, is characterized by the intense and quasi constant AlO_2^- signal whereas Al_2^- and Cu^-, which are characteristic signals of the metallic substrate, remain low. This region is assigned to the outer Al oxide layer. The CuO^- signal remains weak in this region indicating that the oxide is mostly composed of aluminium oxide. As soon as one probes deeper into the substrate, one enters a second region that corresponds to the progressive decrease of the AlO_2^- signal concomitantly with the progressive increase of the Al_2^- and Cu^- signals. After 280s of sputtering, the Cu^- signal reach a maximum intensity, whereas Al_2^- signal continues to increase. This suggest that the metal/oxide interface, which is enriched in Cu, is located at ~280s of sputtering (see dash line on the Figure 2). Thus, the region ranging between 100s and 280s of sputtering, is assigned to an interfacial region that corresponds to both the Al oxide and metallic substrate due to the metal/oxide interface roughness. Finally, the third region, after 280s of sputtering (i.e. metal/oxide interface), is assigned to the metallic substrate. Thus, the sample is mainly composed of metallic aluminium enriched with copper at the metal/oxide interface and covered with aluminium oxide.

This metallic copper enrichment at the metal/oxide interface has been previously observed.[29] Moreover, it is interesting to note that the CuO^- signal is detected on the depth profile (Figure 2 : General ion depth profile recorded on Al-Cu2.2at% alloy, extracted from the 3D ToF-SIMS measurements (Dash lines show oxide/metal interface). Figure 2) in the surface region and remains quasi constant in the other regions contrary to the Cu^- signal. For further verification, the 2D chemical images, extracted from the 3D analysis, are shown in Figure 3 and present essentially the same result.

On the 2D chemical images, the intensity of the detected fragments is dependent on the concentration. Figure 3 shows the 10x10µm² chemical images (Cu^-, CuO^-, AlO_2^-, and Al_2^- ions) obtained by summing stacks of 2D images. Thus in (a) the images of the oxide layer correspond to the sum of the 2D images recorded from 0s to 100s of sputtering, in (b) the images of the interfacial zone correspond to the sum of 2D images recorded between 100 and 280s of sputtering, and in (c) the images of the metallic substrate correspond to the sum of the 2D images recorded from 280s of sputtering to the end. In the oxide layer, as expected, the images show an intense AlO_2^- signal whereas no Cu^-, CuO^-, and Al_2^- signals are detected. This oxide film corresponds to an homogenous aluminium native oxide film. Deeper into the substrate, i.e. in the interfacial region, the AlO_2^- signal remains intense and Al_2^- low (but more intense than

in the oxide layer), indicating that in this interfacial region both oxide and metallic substrate are observed as a result of the interface roughness. Locally Cu^- signals are observed. These Cu^- rich regions also correspond to regions with weak CuO^- intensity (see circled areas on Figure 3b). Moreover, these areas rich in Cu have approximately the same size as the θ-Al_2Cu particles evidenced by SEM. Thus, the Cu-rich areas are assigned to the copper-containing intermetallic particles that are located at the metal/oxide interface and protrude into the oxide film as previously observed.[29] The presence of CuO^- signal, although weak, on these Cu-rich areas suggests that IMPs are, at least partially, oxidized at their surfaces. In the third region (Figure 3c), the Al_2^- ion signal has a high intensity whereas AlO_2^- intensity is weaker (the AlO_2^- signal remains visible in the metallic substrate due to the possible reoxidation of the surface inside the ToF-SIMS main chamber). This confirms that this third region corresponds to the metallic substrate. A Cu^- signal is still visible (at the same location at the one observed previously at the interface (Figure 3b)), but CuO^- is no longer detected in the metallic substrate, indicating that oxidized Cu is only present at the surface of IMPs.

To investigate further the differences between the substrate matrix and IMPs, ToF-SIMS ion depth profiles on top of each region were reconstructed from the raw data by selecting the copper-rich zones, assigned to IMPs (see circled areas on Figure 4a), and the Al matrix (excluding circled areas on Figure 4a). Ion depth profiles on matrix region and IMP region are shown on Figure 4b and Figure 4c, respectively.

The depth profile obtained on the Al matrix (Figure 4b) is globally similar to the one obtained on the global surface (Figure 2). However, it is interesting to note that the I_{Cu^-} / I_{Al2^-} ratio is higher at the metal/oxide interface (~280s of sputtering) than deeper in the bulk, indicating a copper enrichment of the matrix at the metal/oxide interface. This is assigned to the preferential oxidation of the Al as already discussed.[29] This Cu enrichment of the matrix at the metal/oxide interface has been previously predicted by computational work[40], where the authors concluded that the presence of oxide could favour Cu segregation at the matrix/oxide interface. Thus, the matrix is mainly composed of metallic aluminium, enriched with copper at the metal/oxide interface, and is covered by an aluminium oxide layer.

Figure 4c shows an ion depth profile extracted from the IMP zones only. Similarly, the Cu^- signal reaches its maximum at the metal/oxide interface, but a more detailed examination on the depth profile shows that the Cu^- signal reaches its maximum intensity after ~250s of sputtering whereas the metal/oxide interface is located at 280s of sputtering. This confirms that

IMPs located at the metal/oxide interface protrude into the oxide layer, meaning that a thinner oxide is formed on top of the IMPs, with respect to the one formed on the matrix. The Cu-enrichment at the metal/oxide interface and the presence of aluminium oxide over IMPs have been observed previously on Al-Cu alloys[29]. The CuO^- signal in Figure 4c shows a shoulder at the same position as the Cu^- signal which implies that the IMPs are also covered by some copper oxide.

The presence of copper oxide covering the IMPs seems contrary to the thermodynamics. Indeed, as long as the IMP contains sufficiently high metallic aluminium concentration, the thermodynamic predicts that only an aluminium oxide can grow under the oxide layer (at the oxide/metal interface). However, the intermetallic particle could be depleted in aluminium due to its preferential oxidation. Thus, this leads to a copper enrichment on top of the IMPs allowing the formation of copper oxide on top of the particles. This interpretation seems to be confirmed by Figure 4c: the increase of Al_2^- signal intensity is shifted to longer sputtering time (i.e. deeper with respect to the surface) whereas the Cu^- signal intensity is high. This indicates an Al depletion and a copper enrichment at the IMP surface. allowing copper oxidation to occur.

The oxide layer thickness above the intermetallic particles can be evaluated by the detection of the metallic copper on the successive 2D images recorded at different depths (Figure 3) and the depth profiles obtained on the IMPs and matrix areas (Figure 4b and c). It appears that the thickness of the oxide layer covering the IMP is approximately 62% of the thickness of the oxide layer covering the matrix.

The use of ToF-SIMS 3D imaging has allowed us to show that the intermetallic particles are present at the metal/oxide interface and are protruding into the oxide leading to a thinner oxide above IMPs. Although an aluminium oxide covers the entire surface of the sample, copper oxide is detected on top of the IMPs. It is well known that during ToF-SIMS analyses, the changes in ion intensities with the sputtering time are strongly dependent on the matrix from which the ions are emitted[41]. ToF-SIMS depth profiles can also be affected by differential sputtering that can come from the presence of heterogeneities on the surface or the chemical stability of surface species. However, the composition of the oxide scale is quasi homogeneous and mainly consists of Al oxide/hydroxide. Thus, no differential sputtering was considered in the ToF-SIMS depth profiles of the surface oxides. Moreover, the Al oxide/hydroxide is very stable ($\Delta G = -918.4$ kJ/mol) and it is assumed that it is not significantly affected by differential sputtering. It is also noted that the sputter rate changes when passing the oxide-metal interface.

Thus, quantitative analysis by ToF-SIMS is precluded, and XPS analysis is required to obtain quantitative information on the chemical composition.

3.3 Quantitative analysis of the surface composition by XPS

3.3.1 Surface chemical composition

XPS spectra recorded on AlCu2.2at% sample are shown in Figure 5. The main elements on the surface (Figure 5a) are aluminium, carbon, oxygen and copper (weak signal). The Al2p core level spectrum (Figure 5b) is not used to characterize the surface due to an overlap between Al2p and Cu3p[42]. The Al2s core level region (Figure 5c) is decomposed into three peaks at binding energies of 118.2eV (metallic aluminium) and 121.0eV (aluminium oxi/hydroxide) and a peak corresponding to Cu3s photoelectrons (at an energy of 123.2eV[43]). The C1s core level spectrum (Figure 5f) presents four components: at 286.7eV (C-C bonds), 288.3 eV (C-O bonds), 290.5 eV (O-C=O bonds) and 291.8 eV (presence of carbonate CO_3^{2-}) .This decomposition is currently used to describe the contamination layer[44–46]. The O1s core level presents a large peak (Figure 5g). It is decomposed into two peaks at 533.0eV and 534.0eV corresponding to oxygen O^{2-} and the presence of a hydroxylated component on the surface and/or oxygen bonded to contamination carbon, respectively.

The $Cu2p_{3/2}$ core level spectrum is decomposed into two peaks corresponding to copper metal Cu^0 at a binding energy of 932.8eV and a peak at an energy of 934.5eV (Figure 5d).[47,48]. In order to determine the copper chemical environment at high binding energy (metallic or oxidized), the copper Auger spectrum was recorded (Figure 5e). The peak has a weak but sufficient intensity to propose a decomposition presented in Figure 6. The Cu*LMM* Auger spectrum has been decomposed using reference line shapes obtained on standard Cu(0), Cu(I) and Cu(II) compounds. The CASA software was used to combine line shapes of the different standard compounds to reproduce the experimental Cu*LMM* Auger spectrum.

The Augers peaks are decomposed as in the Biesinger[49] study and in other works[50–52]. The experimental Auger line is decomposed using Auger lines associated with metallic copper and Cu(I). The Auger line shape of the metallic copper corresponds to the shape of the Auger line recorded on reference metallic copper, and the Auger line shape of the oxidized copper corresponds to the copper Auger line shape for a Cu_2O reference (stable form of Cu(I)). The low signal intensity makes it difficult to adjust the different peaks to the experimental

Auger spectrum. However, the calculation of the modified Auger parameters for each peak gives an energy of 1851.1eV for the peak at low binding energy and 1849.8eV for the peak at high binding energy. The modified Auger parameter value for the low binding energy peak is in very good agreement with metallic copper (1851.2eV)[48,49] and the Auger parameter of the high binding energy peak value is in fair agreement with Cu(I) (1849.2eV). This result indicates that copper is present in metallic form and in oxide form (Cu(I)).

3.3.2 Oxide layer thickness and model of the native oxide

The ToF-SIMS and XPS analyses showed that the Al-Cu alloy surface is covered by an aluminium oxide/hydroxide layer. Some copper oxide is also present at the surface of the IMPs which are protruding into the oxide. The oxide present above the IMPs is therefore thinner than on the matrix. The first step to evaluate the oxide thickness is to determine the coverage (γ) of IMPs on the surface. The data obtained by ToF-SIMS and SEM allow us to calculate a particle coverage from images by measuring the areas where metallic copper signal is intense. The coverage γ is evaluated at 3.2% of the surface analysed by ToF-SIMS 2D images and 3.4% by SEM images. These results are very close, and in good agreement with the literature which indicates that intermetallic particles typically represent between 2 and 4% of aluminium-copper alloys[2,6,53].

The low coverage allows us to assume that the surface is mainly composed of aluminium and to determine an average oxide thickness above the matrix by neglecting copper. Assuming a simple model consisting of a metallic aluminium substrate covered with uniform and continuous oxide-hydroxide layer (with a uniform surface contamination layer (c)), the equivalent thicknesses of the oxide layer (and of the contamination layer) are determined by XPS analysis. The d_{ox} oxide thickness (and d_c contamination layer) thicknesses are evaluated at 3.5nm (and 0.5nm). This value is in good agreement with the literature for a native oxide whose thickness is usually between 2 and 4 nm on aluminium[54,55].

In order to characterize the oxide present above the IMP, it is necessary to take into account the Cu_2O copper oxide present on top of the IMP, as shown by ToF-SIMS analyses. Thus the real oxide layer is not homogeneous, and it comprises, on the matrix, an aluminium oxy-hydroxide layer and, on the IMPs, aluminium oxide and copper oxide (Cu_2O) islands. The presence of the copper oxide has already been discussed in the previous section. Copper oxide can grow on IMPs if IMPs are covered by an aluminium oxide layer sufficiently thick to deplete

aluminium at the IMP interface. The model based on the above findings is shown in Figure 7. The ToF-SIMS 2D images have provided an IMP coverage γ of 3.2% (in good agreement with the SEM data). In the same way, by measuring the areas where copper oxide signal is intense on the ToF-SIMS images, the coverage γ' of copper oxide islands can be evaluated on the particles. It appears that γ' is about 2.5% of the total image. With γ equal to 3.2% of the total surface, the IMPs are therefore covered by 78% copper oxide. In order to evaluate the hypothesis of a non-homogeneous oxide layer, the copper oxide thickness is calculated taking into account the local model on top of IMPs (see Figure 7). This model is based on several hypotheses. Firstly, all the detected metallic copper signal is assumed to come from the Al_2Cu intermetallic particles and all the Cu_2O oxide signal from the islands. Then, the IMPs are considered thick enough to not detect by XPS the metallic aluminium below. This hypothesis is justified by the SEM analysis which determined that the particles are bigger than the maximum XPS depth of analysis (~10 nm). It is also assumed that the contamination layer present at the surface is homogeneous. Further, the aluminium oxide layer thickness (d'_{ox}) on the IMP surface is set at 62% of the total d_{ox} oxide layer thickness, as evaluated by ToF-SIMS. Finally, copper oxide islands are considered as layers of finite thickness d'. The peak intensity corresponding to copper in the IMPs and the peak intensity corresponding to copper in the oxide copper can therefore be expressed as follows:

$$I_{Cu}^{Al2Cu} = \gamma\, kA(\theta) FT_{Cu}\sigma_{Cu}\lambda_{Cu}^{Al2Cu}D_{Cu}^{Al2Cu} * \sin\theta \left[(1-\gamma')\exp\left(\frac{-d'_{ox}}{\lambda_{Cu}^{Al2O3}sin\theta}\right) + \gamma'\exp\left(\frac{-d'}{\lambda_{Cu}^{Cu2O}sin\theta}\right) * \exp\left(\frac{-(d'_{ox}-d')}{\lambda_{Cu}^{Al2O3}sin\theta}\right)\right] * \exp\left(\frac{-d_c}{\lambda_{Cu}^{c}sin\theta}\right)$$

$$I_{Cu}^{Cu2O} = \gamma\, kA(\theta) FT_{Cu}\sigma_{Cu}\lambda_{Cu}^{Cu2O}D_{Cu}^{Cu2O}sin\theta\gamma'\left[1-\exp\left(\frac{-d'}{\lambda_{Cu}^{Cu2O}sin\theta}\right)\right] * \exp\left(\frac{-(d'_{ox}-d')}{\lambda_{Cu}^{Al2O3}sin\theta}\right) * \exp\left(\frac{-d_c}{\lambda_{Cu}^{c}sin\theta}\right)$$

with I_X^Y the intensity of photoelectrons emitted by the element X (in the considered core level) in the matrix Y, $kA(\theta)$ a constant characteristic of the spectrometer, σ_X the photoionization cross-section of the core level of the element X, λ_X^Y the inelastic mean free path of photoelectrons emitted by the core level of the element X in the matrix Y, D_X^Y the density of the element X in the matrix Y, T_X the transmission function of the core level of the element X, d the thickness for the carbon contamination (d_c), the oxide layer present on the matrix surface (d_{ox}), the oxide layer present on the IMP surface (d'_{ox}) and the copper oxide layer d' on the IMP.

The ratio of these two equations gives the thickness, d', of the copper oxide islands. The thickness is evaluated at 0.5nm, knowing the aluminium oxide layer on the intermetallic is estimated at 2.2 nm (d'_{ox}). This value is consistent with the small amount of copper oxide detected by XPS and ToF-SIMS on the alloy surface. The model of the native oxide layer on the Al-Cu alloy, based on XPS and ToF-SIMS analyses, is shown on Figure 7.

These results are consistent with those obtained recently by Li *et al.*[25], who studied the differences of initial growth of the passive films between Al matrix and Al_2CuMg particles on an AA2024-T3 aluminium alloy. They found by XPS and AES depth profiles that the oxide layer on Al_2CuMg particles is thinner that the one on the Al matrix (1.4nm versus 2.4 nm), and not composed only of aluminium oxide but also of copper oxide. The atomic ratio of Cu/Al at the interface was larger than that in the substrate, which suggested that there was Cu enrichment at the Al_2CuMg/oxide interface.

Others authors, as Frankel *et al.*[11,56,57] reported lateral heterogeneities within particles. In particular, Zhu *et al.*[12] using APT and SKPFM, studied the intermetallic compounds in AA2070-T8 and showed that intermetallic particles are not homogeneous and present lateral distribution of the potential implying the segregation of heavy elements (i.e. Cu in Al_2Cu particles).

4. Conclusions

The AlCu2.2%at model alloy, containing only one type of intermetallic particles (Al_2Cu), has been characterized by the combination of ToF-SIMS and XPS analyses. The analyses revealed that these particles are present at the metal/oxide interface with a surface coverage of 3.2%. The oxide layer, mostly composed of aluminium oxide/hydroxide and a small amount of Cu(I) oxide, is not homogeneous. Differences in thickness and composition occur depending on the underlying material composition. An aluminium oxide/hydroxide approximately 3nm thick covers the aluminium matrix, with copper enrichment at the metal/oxide interface. The oxide layer is thinner above the IMPs protruding into the oxide layer. The presence of copper oxide islands on the IMPs was revealed. They are approximately 0.5nm thick and the surface coverage is approximately 2.5% of the total surface. The oxide thickness above the IMPs is 2.2nm. A model of the native oxide layer on the Al-Cu alloy surface incorporating the above features has been proposed. The different types of heterogeneities identified in the present work can influence the cathodic or anodic character of the surface.[58]

To rationalize the effect of each parameter (oxide thickness, composition, Cu enrichment) on the corrosion resistance, DFT-based models of the different zones of the matrix and the IMP will be built and analysed in our future work.

Acknowledgements

Région Ile de France is acknowledged for partial funding of the XPS and ToF-SIMS equipments. Pauline Cornette thanks the doctoral school ED388 (UPMC and PSL) for a PhD grant.

The authors declare no conflict of interest.

The raw/processed data required to reproduce these findings cannot be shared at this time due to technical or time limitations.

5. References

[1] C. Vargel, Corrosion of aluminium, 1st ed, Elsevier, Amsterdam ; Boston, 2004.
[2] T.H. Muster, A.E. Hughes, G.E. Thompson, Copper distributions in aluminum alloys, Nova Science Publishers, New York, 2009. http://public.eblib.com/choice/publicfullrecord.aspx?p=3018510 (accessed December 5, 2016).
[3] P. Marcus, ed., Corrosion mechanisms in theory and practice, 3rd ed, CRC Press, Boca Raton, 2012.
[4] V. Guillaumin, G. Mankowski, Localized corrosion of 2024 T351 aluminium alloy in chloride media, Corros. Sci. 41 (1998) 421–438. https://doi.org/10.1016/S0010-938X(98)00116-4.
[5] R.G. Buchheit, A Compilation of Corrosion Potentials Reported for Intermetallic Phases in Aluminum Alloys, J. Electrochem. Soc. 142 (1995) 3994. https://doi.org/10.1149/1.2048447.
[6] R.G. Buchheit, R.P. Grant, P.F. Hlava, B. Mckenzie, G.L. Zender, Local Dissolution Phenomena Associated with S Phase (Al2CuMg) Particles in Aluminum Alloy 2024-T3, J. Electrochem. Soc. 144 (1997) 2621–2628. https://doi.org/10.1149/1.1837874.
[7] T. Suter, R.C. Alkire, Microelectrochemical Studies of Pit Initiation at Single Inclusions in Al 2024-T3, J. Electrochem. Soc. 148 (2001) B36. https://doi.org/10.1149/1.1344530.
[8] Zhou, Herong, Yao, Wang, Du, Cuiwei, Song, Shupeng, Wu, Run, Corrosion Behavior of the Al2Cu Intermetallic Compound and Coupled Al2Cu/Al, Int. J. Electrochem. Sci. (2017) 9542–9554. https://doi.org/10.20964/2017.10.32.
[9] G.M. Scamans, N. Birbilis, R.G. Buchheit, Corrosion of Aluminum and its Alloys, in: T Richardson Ed Shreirs Corros., 1st ed., Elsevier, The Netherlands, 2010: pp. 1974–2010. https://doi.org/10.1016/B978-044452787-5.00095-0.
[10] C. Örnek, C. Leygraf, J. Pan, On the Volta potential measured by SKPFM – fundamental and practical aspects with relevance to corrosion science, Corros. Eng. Sci. Technol. 54 (2019) 185–198. https://doi.org/10.1080/1478422X.2019.1583436.

[11] P. Schmutz, Frankel, GS., Characterization of AA2024-T3 by Scanning Kelvin Probe Force Microscopy, J. Electrochem. Soc. 145 (1998) 2285. https://doi.org/10.1149/1.1838633.
[12] Y. Zhu, K. Sun, J. Garves, L.G. Bland, J. Locke, J. Allison, G.S. Frankel, Micro- and nano-scale intermetallic phases in AA2070-T8 and their corrosion behavior, Electrochimica Acta. 319 (2019) 634–648. https://doi.org/10.1016/j.electacta.2019.05.028.
[13] G.S. Chen, M. Gao, R.P. Wei, Microconstituent-Induced Pitting Corrosion in Aluminum Alloy 2024-T3, CORROSION. 52 (1996) 8–15. https://doi.org/10.5006/1.3292099.
[14] J.R. Scully, T.O. Knight, R.G. Buchheit, D.E. Peebles, Electrochemical characteristics of the Al2Cu, Al3Ta and Al3Zr intermetallic phases and their relevancy to the localized corrosion of Al alloys, Corros. Sci. 35 (1993) 185–195. https://doi.org/10.1016/0010-938X(93)90148-A.
[15] J.R. Scully, D.E. Peebles, A.D. Romig, D.R. Frear, C.R. Hills, Metallurgical factors influencing the corrosion of aluminum, Al-Cu, and Al-Si alloy thin films in dilute hydrofluoric solution, Metall. Trans. A. 23 (1992) 2641–2655. https://doi.org/10.1007/BF02658068.
[16] G.O. Ilevbare, O. Schneider, R.G. Kelly, J.R. Scully, In Situ Confocal Laser Scanning Microscopy of AA 2024-T3 Corrosion Metrology, J. Electrochem. Soc. 151 (2004) B453. https://doi.org/10.1149/1.1764780.
[17] A.E. Hughes, R. Parvizi, M. Forsyth, Microstructure and corrosion of AA2024, Corros. Rev. 33 (2015) 1–30. https://doi.org/10.1515/corrrev-2014-0039.
[18] A.E. Hughes, A. Boag, A.M. Glenn, D. McCulloch, T.H. Muster, C. Ryan, C. Luo, X. Zhou, G.E. Thompson, Corrosion of AA2024-T3 Part II: Co-operative corrosion, Corros. Sci. 53 (2011) 27–39. https://doi.org/10.1016/j.corsci.2010.09.030.
[19] P. Carbonini, T. Monetta, D.B. Mitton, F. Bellucci, P. Mastronardi, B. Scatteia, Degradation behaviour of 6013-T6, 2024-T3 alloys and pure aluminium in different aqueous media, J. Appl. Electrochem. 27 (1997) 1135–1142. https://doi.org/10.1023/A:1018459214994.
[20] M. Schneider, O. Yezerska, M.M. Lohrengel, Anodic oxide formation on AA2024: electrochemical and microstructure investigation, Corros. Eng. Sci. Technol. 43 (2008) 304–312. https://doi.org/10.1179/174327808X286211.
[21] M. Saenz de Miera, M. Curioni, P. Skeldon, G.E. Thompson, Preferential anodic oxidation of second-phase constituents during anodising of AA2024-T3 and AA7075-T6 alloys, Surf. Interface Anal. 42 (2010) 241–246. https://doi.org/10.1002/sia.3191.
[22] L. Marín, C.E. Nanayakkara, J.-F. Veyan, B. Warot-Fonrose, S. Joulie, A. Estève, C. Tenailleau, Y.J. Chabal, C. Rossi, Enhancing the Reactivity of Al/CuO Nanolaminates by Cu Incorporation at the Interfaces, ACS Appl. Mater. Interfaces. 7 (2015) 11713–11718. https://doi.org/10.1021/acsami.5b02653.
[23] L. Marín, B. Warot-Fonrose, A. Estève, Y.J. Chabal, L. Alfredo Rodriguez, C. Rossi, Self-Organized Al2Cu Nanocrystals at the Interface of Aluminum-Based Reactive Nanolaminates to Lower Reaction Onset Temperature, ACS Appl. Mater. Interfaces. 8 (2016) 13104–13113. https://doi.org/10.1021/acsami.6b02008.
[24] A. Seyeux, G.S. Frankel, N. Missert, K.A. Unocic, L.H. Klein, A. Galtayries, P. Marcus, ToF-SIMS Imaging Study of the Early Stages of Corrosion in Al-Cu Thin Films, J. Electrochem. Soc. 158 (2011) C165–C171. https://doi.org/10.1149/1.3568944.
[25] N. Li, C. Dong, C. Man, J. Yao, In Situ Electrochemical Atomic Force Microscopy and Auger Electro Spectroscopy Study on the Passive Film Structure of 2024-T3 Aluminum Alloy Combined with a Density Functional Theory Calculation, Adv. Eng. Mater. 21 (2019) 1900386. https://doi.org/10.1002/adem.201900386.

[26] K.-A. Son, N. Missert, J.C. Barbour, J.J. Hren, R.G. Copeland, K.G. Minor, Growth and Oxidation of Thin Film Al[sub 2]Cu, J. Electrochem. Soc. 148 (2001) B260. https://doi.org/10.1149/1.1376635.
[27] A. Roberts, D. Engelberg, Y. Liu, G.E. Thompson, M.R. Alexander, Imaging XPS investigation of the lateral distribution of copper inclusions at the abraded surface of 2024T3 aluminium alloy and adsorption of decyl phosphonic acid, Surf. Interface Anal. 33 (2002) 697–703. https://doi.org/10.1002/sia.1441.
[28] M.H. Larsen, J.C. Walmsley, O. Lunder, R.H. Mathiesen, K. Nisancioglu, Intergranular Corrosion of Copper-Containing AA6xxx AlMgSi Aluminum Alloys, J. Electrochem. Soc. 155 (2008) C550. https://doi.org/10.1149/1.2976774.
[29] A. Seyeux, G.S. Frankel, N. Missert, K.A. Unocic, L.H. Klein, A. Galtayries, P. Marcus, ToF-SIMS Imaging Study of the Early Stages of Corrosion in Al-Cu Thin Films, J. Electrochem. Soc. 158 (2011) C165. https://doi.org/10.1149/1.3568944.
[30] S. Tanuma, C.J. Powell, D.R. Penn, Calculations of electron inelastic mean free paths. V. Data for 14 organic compounds over the 50–2000 eV range, Surf. Interface Anal. 21 (1994) 165–176. https://doi.org/10.1002/sia.740210302.
[31] P. Marcus, C. Hinnen, I. Olefjord, Determination of attenuation lengths of photoelectrons in aluminium and aluminium oxide by angle-dependent x-ray photoelectron spectroscopy, Surf. Interface Anal. 20 (1993) 923–929. https://doi.org/10.1002/sia.740201108.
[32] A. Benninghoven, Chemical Analysis of Inorganic and Organic Surfaces and Thin Films by Static Time-of-Flight Secondary Ion Mass Spectrometry (TOF-SIMS), Angew. Chem. Int. Ed. Engl. 33 (1994) 1023–1043. https://doi.org/10.1002/anie.199410231.
[33] S.E. Potts, L. Schmalz, M. Fenker, B. Díaz, J. Światowska, V. Maurice, A. Seyeux, P. Marcus, G. Radnóczi, L. Tóth, W.M.M. Kessels, Ultra-Thin Aluminium Oxide Films Deposited by Plasma-Enhanced Atomic Layer Deposition for Corrosion Protection, J. Electrochem. Soc. 158 (2011) C132–C138. https://doi.org/10.1149/1.3560197.
[34] M. Ely, J. Światowska, A. Seyeux, S. Zanna, P. Marcus, Role of Post-Treatment in Improved Corrosion Behavior of Trivalent Chromium Protection (TCP) Coating Deposited on Aluminum Alloy 2024-T3, J. Electrochem. Soc. 164 (2017) C276–C284. https://doi.org/10.1149/2.0431706jes.
[35] B. Díaz, E. Härkönen, J. Światowska, V. Maurice, A. Seyeux, P. Marcus, M. Ritala, Low-temperature atomic layer deposition of Al2O3 thin coatings for corrosion protection of steel: Surface and electrochemical analysis, Corros. Sci. 53 (2011) 2168–2175. https://doi.org/10.1016/j.corsci.2011.02.036.
[36] S. Mirhashemihaghighi, J. Światowska, V. Maurice, A. Seyeux, L.H. Klein, E. Salmi, M. Ritala, P. Marcus, Interfacial native oxide effects on the corrosion protection of copper coated with ALD alumina, Electrochimica Acta. 193 (2016) 7–15. https://doi.org/10.1016/j.electacta.2016.02.014.
[37] S. Mirhashemihaghighi, J. Światowska, V. Maurice, A. Seyeux, S. Zanna, E. Salmi, M. Ritala, P. Marcus, Corrosion protection of aluminium by ultra-thin atomic layer deposited alumina coatings, Corros. Sci. 106 (2016) 16–24. https://doi.org/10.1016/j.corsci.2016.01.021.
[38] R. Viroulaud, J. Światowska, A. Seyeux, S. Zanna, J. Tardelli, P. Marcus, Influence of surface pretreatments on the quality of trivalent chromium process coatings on aluminum alloy, Appl. Surf. Sci. 423 (2017) 927–938. https://doi.org/10.1016/j.apsusc.2017.06.246.
[39] J. Mosa, N. C. Rosero-Navarro, M. Aparicio, Active corrosion inhibition of mild steel by environmentally-friendly Ce-doped organic–inorganic sol–gel coatings, RSC Adv. 6 (2016) 39577–39586. https://doi.org/10.1039/C5RA26094A.

[40] P. Cornette, D. Costa, P. Marcus, DFT Modelling of Cu Segregation in Al-Cu Alloys Covered by an Ultrathin Oxide Film and Possible Links with Passivity, Metals. 7 (2017) 366. https://doi.org/10.3390/met7090366.
[41] J. Grams, New trends and potentialities of ToF-SIMS in surface studies, Nova Science Publishers, New York, 2007.
[42] C.D. Wagner, G.E. Muilenberg, W.M. Riggs, L.E. Davis, J.F. Moulder, Handbook of X-ray photoelectron spectroscopy, Perkin-Elmer, Eden Prairie, Minn, 1979.
[43] G. Johansson, J. Hedman, A. Berndtsson, M. Klasson, R. Nilsson, Calibration of electron spectra, J. Electron Spectrosc. Relat. Phenom. 2 (1973) 295–317. https://doi.org/10.1016/0368-2048(73)80022-2.
[44] E. McCafferty, J.P. Wightman, Determination of the concentration of surface hydroxyl groups on metal oxide films by a quantitative XPS method, Surf. Interface Anal. 26 (1998) 549–564. https://doi.org/10.1002/(SICI)1096-9918(199807)26:8<549::AID-SIA396>3.0.CO;2-Q.
[45] D. Mercier, J.-C. Rouchaud, M.-G. Barthés-Labrousse, Interaction of amines with native aluminium oxide layers in non-aqueous environment: Application to the understanding of the formation of epoxy-amine/metal interphases, Appl. Surf. Sci. 254 (2008) 6495–6503. https://doi.org/10.1016/j.apsusc.2008.04.010.
[46] J. van den Brand, W.G. Sloof, H. Terryn, J.H.W. de Wit, Correlation between hydroxyl fraction and O/Al atomic ratio as determined from XPS spectra of aluminium oxide layers, Surf. Interface Anal. 36 (2004) 81–88. https://doi.org/10.1002/sia.1653.
[47] N.S. McIntyre, M.G. Cook, X-ray photoelectron studies on some oxides and hydroxides of cobalt, nickel, and copper, Anal. Chem. 47 (1975) 2208–2213. https://doi.org/10.1021/ac60363a034.
[48] G. Deroubaix, P. Marcus, X-ray photoelectron spectroscopy analysis of copper and zinc oxides and sulphides, Surf. Interface Anal. 18 (1992) 39–46. https://doi.org/10.1002/sia.740180107.
[49] M.C. Biesinger, L.W.M. Lau, A.R. Gerson, R.St.C. Smart, Resolving surface chemical states in XPS analysis of first row transition metals, oxides and hydroxides: Sc, Ti, V, Cu and Zn, Appl. Surf. Sci. 257 (2010) 887–898. https://doi.org/10.1016/j.apsusc.2010.07.086.
[50] B.E. Torres Bautista, A.J. Wikieł, I. Datsenko, M. Vera, W. Sand, A. Seyeux, S. Zanna, I. Frateur, P. Marcus, Influence of extracellular polymeric substances (EPS) from Pseudomonas NCIMB 2021 on the corrosion behaviour of 70Cu–30Ni alloy in seawater, J. Electroanal. Chem. 737 (2015) 184–197. https://doi.org/10.1016/j.jelechem.2014.09.024.
[51] B.R. Strohmeier, D.E. Levden, R.S. Field, D.M. Hercules, Surface spectroscopic characterization of CuAl2O3 catalysts, J. Catal. 94 (1985) 514–530. https://doi.org/10.1016/0021-9517(85)90216-7.
[52] C.E. Moffitt, D.M. Wieliczka, H.K. Yasuda, An XPS study of the elemental enrichment on aluminum alloy surfaces from chemical cleaning, Surf. Coat. Technol. 137 (2001) 188–196. https://doi.org/10.1016/S0257-8972(00)01121-X.
[53] M.A. Jakab, D.A. Little, J.R. Scully, Experimental and Modeling Studies of the Oxygen Reduction Reaction on AA2024-T3, J. Electrochem. Soc. 152 (2005) B311–B320. https://doi.org/10.1149/1.1949047.
[54] C. Vargel, Corrosion de l'aluminium, Dunod, Paris, 1999.
[55] I. Olefjord, H.J. Mathieu, P. Marcus, Intercomparison of surface analysis of thin aluminium oxide films, Surf. Interface Anal. 15 (1990) 681–692. https://doi.org/10.1002/sia.740151108.

[56] P. Leblanc, G.S. Frankel, A Study of Corrosion and Pitting Initiation of AA2024-T3 Using Atomic Force Microscopy, J. Electrochem. Soc. 149 (2002) B239. https://doi.org/10.1149/1.1471546.
[57] V. Guillaumin, P. Schmutz, G.S. Frankel, Characterization of Corrosion Interfaces by the Scanning Kelvin Probe Force Microscopy Technique, J. Electrochem. Soc. 148 (2001) B163. https://doi.org/10.1149/1.1359199.
[58] C. Örnek, M. Liu, J. Pan, Y. Jin, C. Leygraf, Volta Potential Evolution of Intermetallics in Aluminum Alloy Microstructure Under Thin Aqueous Adlayers: A combined DFT and Experimental Study, Top. Catal. 61 (2018) 1169–1182. https://doi.org/10.1007/s11244-018-0939-9.

Figure:

Figure 1 : SEM image obtained on model Al-Cu2.2 at% alloy. The lighter areas represent the Al_2Cu intermetallic particles.

Figure 2 : General ion depth profile recorded on Al-Cu2.2at% alloy, extracted from the 3D ToF-SIMS measurements (Dash lines show oxide/metal interface).

Figure 3 : ToF-SIMS negative ion images of Cu^-, CuO^-, AlO_2^-, and Al_2^- recorded on Al-Cu2.2at% alloy surface at different depths: (a) oxide layer region corresponding to the 2D images recorded from 0s to 100s of sputtering, (b) interfacial zone corresponding to the 2D images recorded between 100 and 280s of sputtering, and (c) metallic substrate corresponding to the 2D images recorded from 280s of sputtering to the end. Areas of Cu^- and CuO^- enrichment are circled for clarity.

Figure 4 : ToF-SIMS negative ions analysis: A) Cu^- ion images, θ-Al_2Cu particles are indicated by circled zones. B) depth profiles obtained on the alloy matrix (i.e. by excluding signals from the circled zones on A). Arrows are reported to indicate the copper enrichment at the metal/oxide interface compared to bulk. C) depth profiles obtained from the IMPs of AlCu samples (i.e. by selecting signals from the circled zones on A). Dash lines represent metal/oxide interface.

Figure 5 : XPS spectra recorded on AlCu2.2 at % sample a) Survey spectrum b) Al2p and Cu3p core level spectrum c) Al2s and Cu3s core level spectrum d) $Cu2p_{3/2}$ core level spectrum e) Cu Auger spectrum f) C1s core level spectrum g) O1s core level spectrum.

Figure 6 : Decomposition of the copper Auger spectrum recorded on AlCu 2.2 at %.

Figure 7 : Model of the native oxide layer on the Al-Cu alloy, based on XPS and ToF-SIMS analyses, with the thickness of the carbon contamination (d_c), the oxide layer present on the Al matrix (d_{ox}), the oxide layer present on the IMP surface (d'_{ox}), the copper oxide layer d' on the IMP and γ the coverage of IMPs on the surface and γ' the coverage of the copper oxide island on the surface.

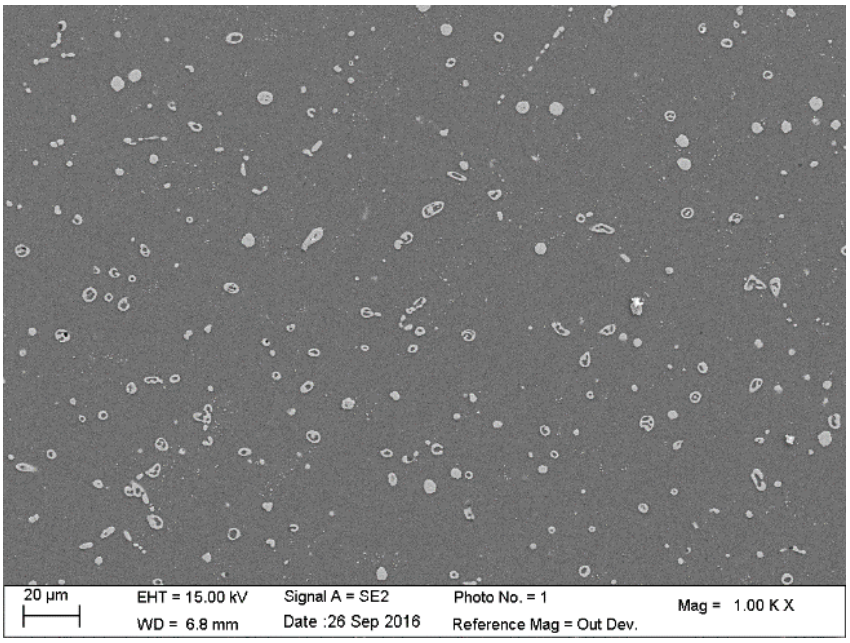

Figure 1 : SEM image obtained on model Al-Cu2.2 at% alloy. The lighter areas represent the Al_2Cu intermetallic particles.

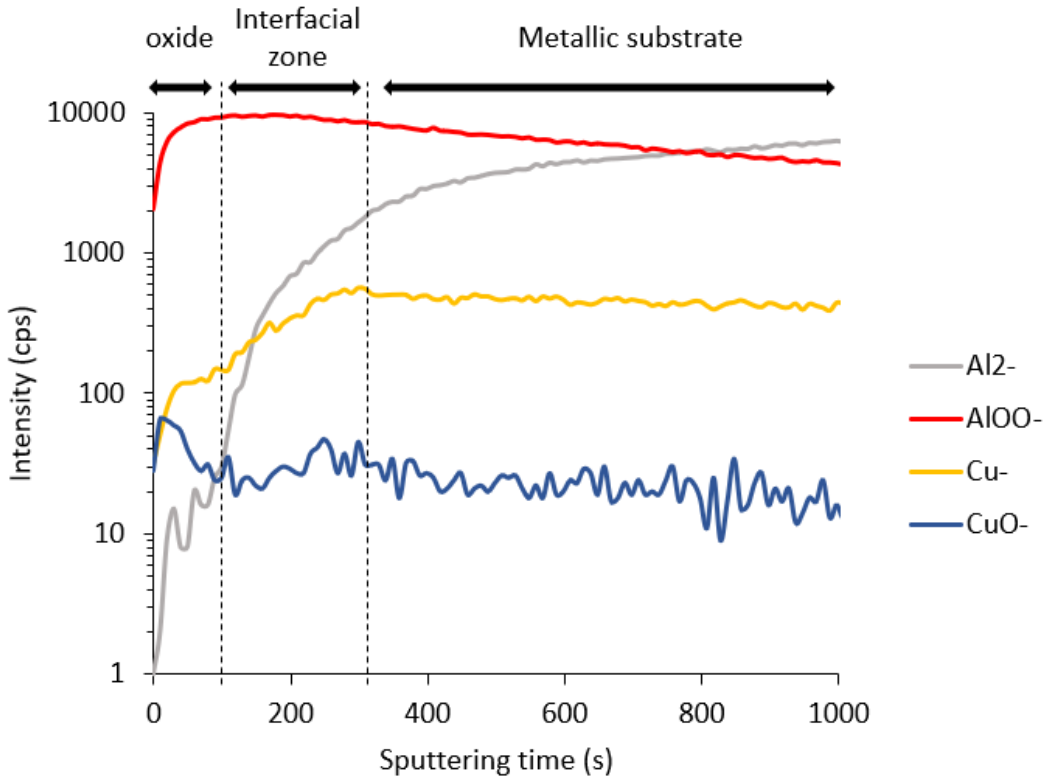

Figure 2 : General ion depth profile recorded on Al-Cu2.2at% alloy, extracted from the 3D ToF-SIMS measurements (Dash lines show oxide/metal interface).

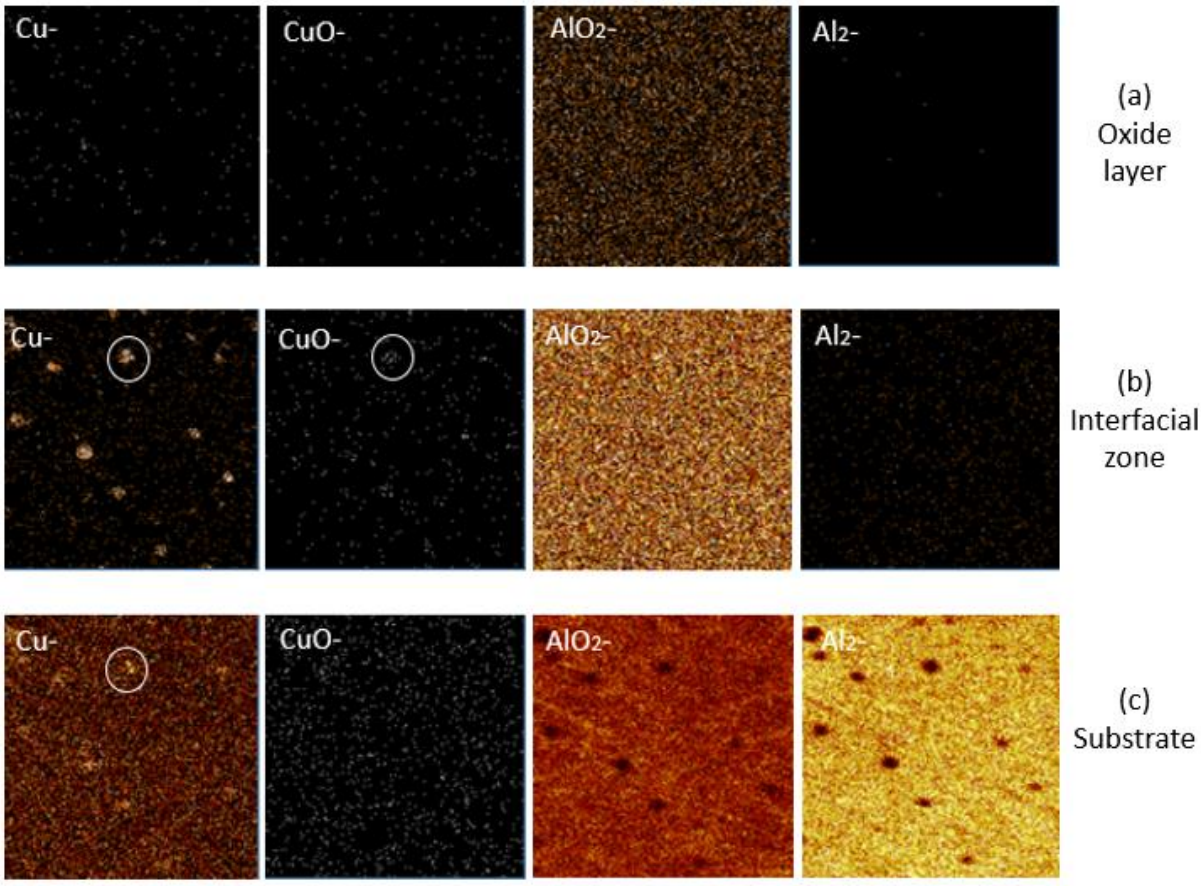

Figure 3 : ToF-SIMS negative ion images of Cu^-, CuO^-, AlO_2^-, and Al_2^- recorded on Al-Cu2.2at% alloy surface at different depths: (a) oxide layer region corresponding to the 2D images recorded from 0s to 100s of sputtering, (b) interfacial zone corresponding to the 2D images recorded between 100 and 280s of sputtering, and (c) metallic substrate corresponding to the 2D images recorded from 280s of sputtering to the end. Areas of Cu^- and CuO^- enrichment are circled for clarity.

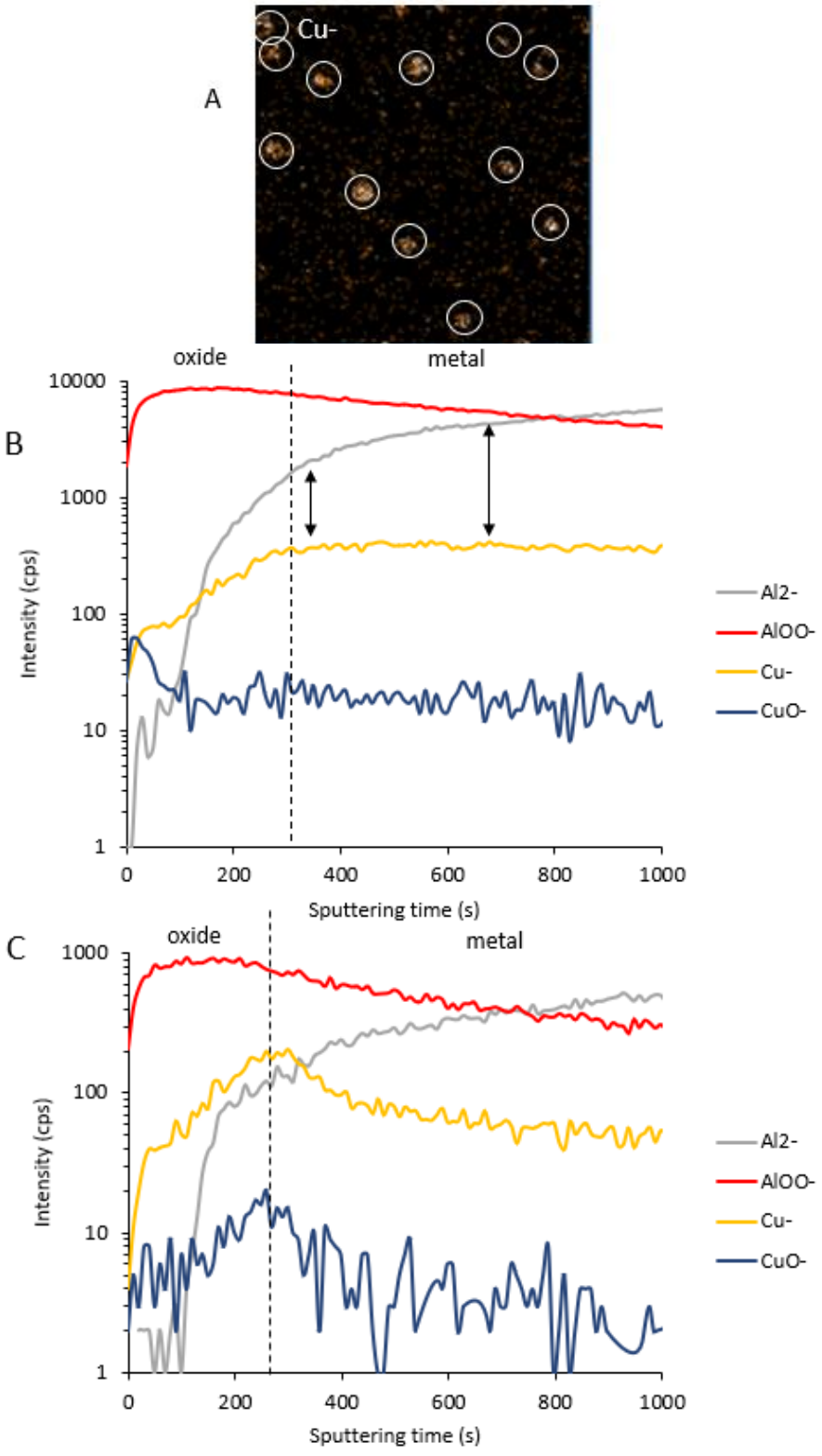

Figure 4 : ToF-SIMS negative ions analysis: A) Cu^- ion images, θ-Al_2Cu particles are indicated by circled zones. B) depth profiles obtained on the alloy matrix (i.e. by excluding signals from the circled zones on A). Arrows are reported to indicate the copper enrichment at the metal/oxide interface compared to bulk. C) depth profiles obtained from the IMPs of AlCu samples (i.e. by selecting signals from the circled zones on A). Dash lines represent metal/oxide interface.

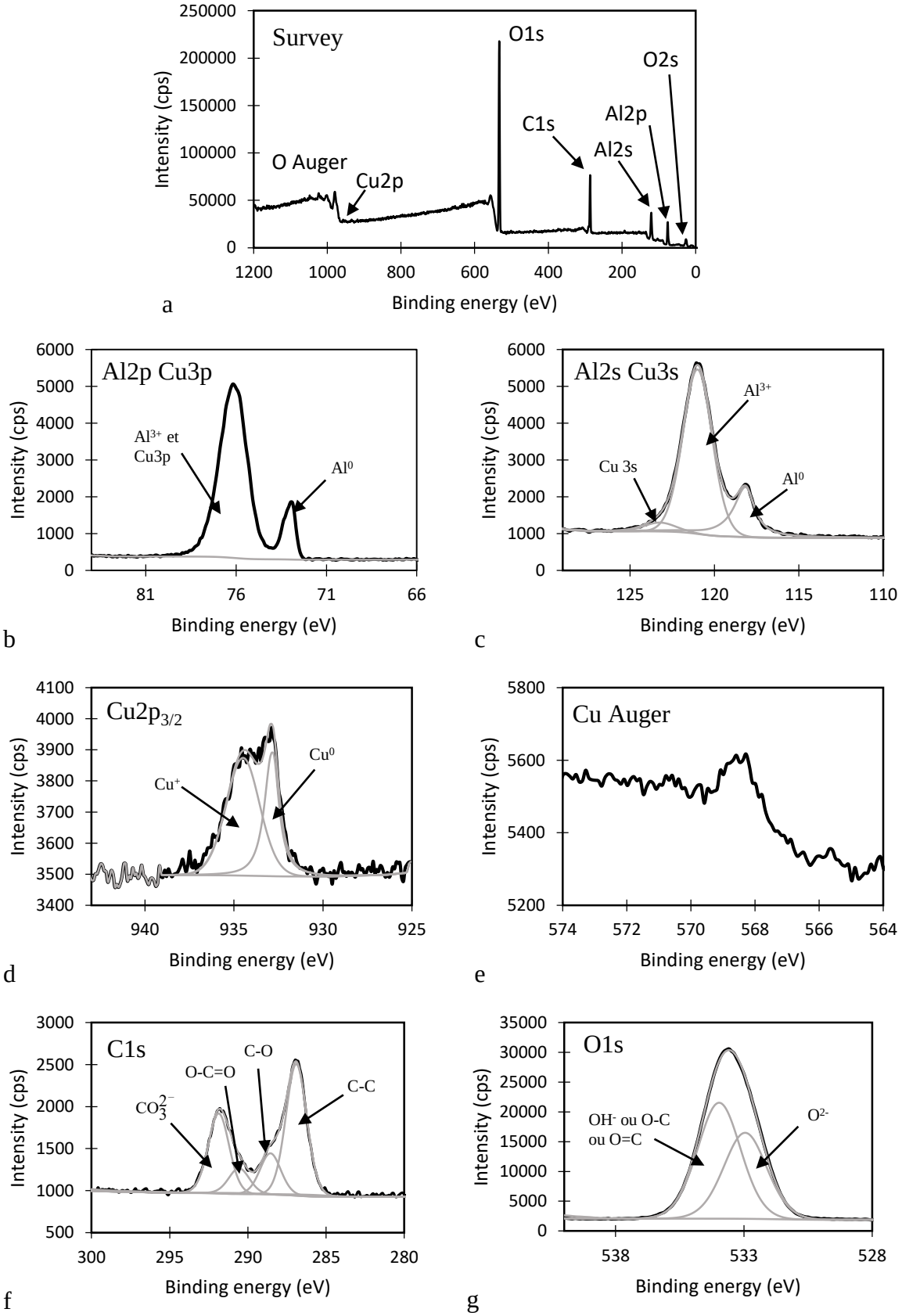

Figure 5 : XPS spectra recorded on AlCu2.2 at % sample a) Survey spectrum b) Al2p and Cu3p core level spectrum c) Al2s and Cu3s core level spectrum d) $Cu2p_{3/2}$ core level spectrum e) Cu Auger spectrum f) C1s core level spectrum g) O1s core level spectrum.

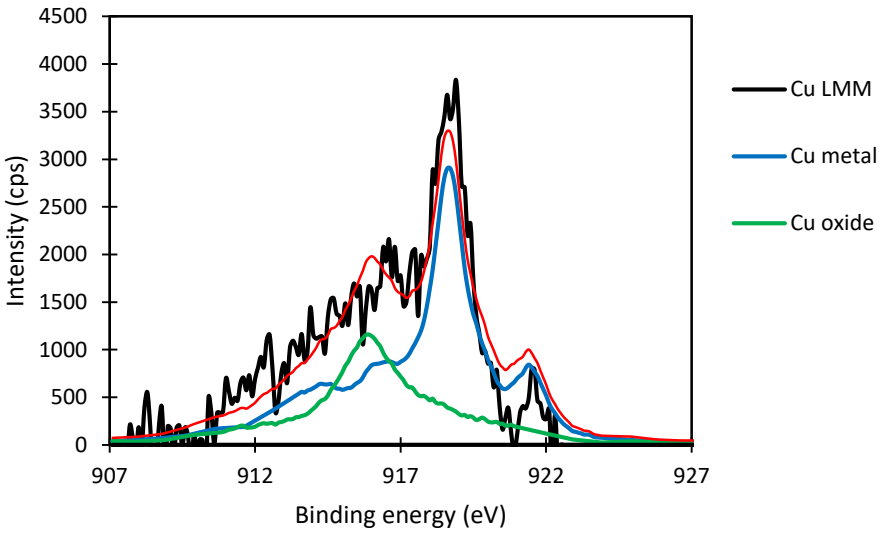

Figure 6 : Decomposition of the copper Auger spectrum recorded on AlCu 2.2 at %.

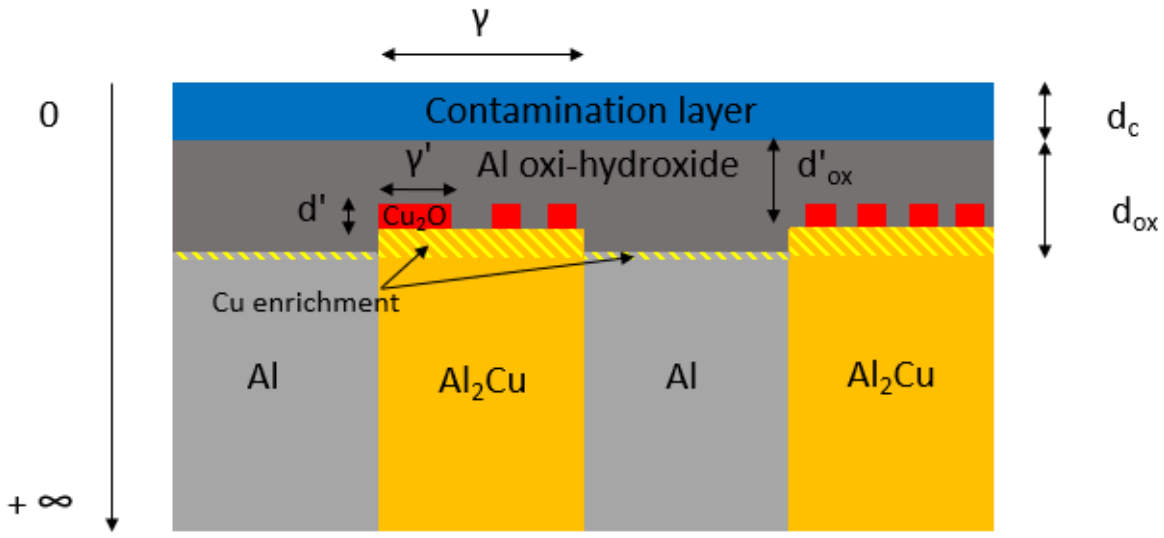

Figure 7 : Model of the native oxide layer on the Al-Cu alloy, based on XPS and ToF-SIMS analyses, with the thickness of the carbon contamination (d_c), the oxide layer present on the Al matrix (d_{ox}), the oxide layer present on the IMP surface (d'_{ox}), the copper oxide layer d' on the IMP and γ the coverage of IMPs on the surface and γ' the coverage of the copper oxide island on the surface.